Early-Stage Fault Diagnosis for Rotating Element Bearing Using Improved Harmony Search Algorithm With Different Fitness Functions

Muhammad Ahsan and Dariusz Bismor, *Senior Member, IEEE*

***Abstract*— Bearings are the backbone of every rotary machine that ranges from civilian to military applications. A single fault in a bearing can shut down the whole machine that causes personal damage and economic loss. To prevent the sudden shut down of rotating machines, signal processing techniques are used to find out the early-stage faults. In this article, a new early-stage fault detection algorithm is proposed that uses the harmony search (HS) algorithm to determine the optimum fault frequency spectrum. For that, a bandpass filter is applied to the vibration signal, and the parameters of the bandpass filter such as center frequency, bandwidth, and order of the filter are dynamic and depend on the type of faults and the fault frequency resonance band. To estimate the dynamic parameters of the bandpass filter, different fitness functions are used based on kurtosis and spectrum kurtosis. The fitness functions of the optimum fault frequency spectrum have the highest value compared to the healthy frequency spectrum. The proposed method is fully data-driven, and the HS algorithm is employed to optimize the parameters of the bandpass filter. The results of the proposed method have been compared with the fast kurtogram, and it has been concluded that the bandpass filter designed using the HS algorithm has a better performance. To validate the proposed method, two datasets are employed and the simulation results are obtained using the MATLAB environment.**

***Index Terms*— Early-stage fault, fast kurtogram, harmony search (HS) algorithm, short-time Fourier transform (STFT), signal processing, spectral kurtosis (SK).**

I. Introduction

EVERY rotary machine is composed of bearings that range from civilian to military applications, such as motors, industrial fans, compressors, automobiles, turbines, and vehicles [1]–[4]. A single fault in a bearing can shut down the whole machine it is contained within; therefore, vibration analysis techniques are extensively studied to detect early-stage faults in rotary machines [5], [6]. Predictive maintenance of rotating machines in the modern industry can nullify the failure in rolling element bearings that results in both economic loss and personal damage.

Based on sensor properties, different methods are used to compute the faults, such as current-based methods, torque-based methods, sound-based methods, acoustic emission-based, or vibration-based methods [3], [7]–[9]. The vibration-based methods are extensively researched because the signal generated by the vibration sensors represents the dynamic behavior of a bearing. However, it is a challenging task to accurately detect the fault frequency resonance band because of the unwanted signals and noise. The faulty vibration signal S measured from the rolling element bearing is expressed as follows:

$$S = S_v + S_f + S_n \tag{1}$$

where S_n, S_f, and S_v are the noise signal, periodic signal, and shaft signal, respectively. In reality, a vibration signal measured from a rotary machine consists of many other frequencies along with its shaft rotating frequency [10] and given as follows:

$$S_v = \alpha_1 \cos(2\pi f_1 t) + \alpha_2 \cos(2\pi f_2 t) + \alpha_3 \cos(2\pi f_3 t) \tag{2}$$

where f_1 is the shaft rotating frequency, f_2 and f_3 are the selected harmonics of f_1, and α_1, α_2, and α_3 are the magnitudes of the signals (usually less than one).

The periodic signal occurs due to the faults in the bearing and the purpose of the fault diagnosis is to determine these periodic signals [5]. This is a challenging task as the energy of these faulty signals is very small compared to the total energy of the signal

$$S_f = \sum_k X_k h(t - \tau_k) \tag{3}$$

where $h(t)$ represents the impulse response with a random time of the impacts τ_k and a random sequence of amplitudes X_k. k is the set of real numbers. The rolling elements of the bearing possess random slips and random pulses, and hence it is known as a stochastic process. The resulting signals are pseudo-cyclostationary instead of cyclostationary due to the lack of memory of the previous slips, but are usually treated as cyclostationary [11], [12].

Different signal processing and artificial intelligence methods are used for early-stage fault diagnoses [13]–[17]. Both groups of methods present many challenges, for example, fault frequency detection is difficult for a weak signal with a high level of noise, and for neural network-based AI methods, a large dataset and a substantial amount of time are required for the neural network training [13], [18], [19]. In recent

Manuscript received 31 January 2022; revised 17 June 2022; accepted 1 July 2022. Date of publication 19 July 2022; date of current version 11 August 2022. This work was supported by the State Budget for Science, Poland. The Associate Editor coordinating the review process was Dr. Yuhua Cheng. *(Corresponding author: Muhammad Ahsan.)*

The authors are with the Department of Measurements and Control Systems, Silesian University of Technology, 44-100 Gliwice, Poland (e-mail: ahsanmuhammad@aol.com; dariusz.bismor@polsl.pl).

Digital Object Identifier 10.1109/TIM.2022.3192254

years, many new techniques such as wavelet transform, and so on [13], [15], [20] were developed for the analysis of a rolling element bearing. However, these analysis techniques are subjected to constraints, and diagnosis sensitivity is not much efficient for alternative working conditions. In the literature, envelope analysis is widely applied to detect fault frequencies [21] by calculating the power spectrum density (PSD). Unfortunately, when the signal is exposed to high levels of noise, PSD fails to compute the faults and hence is not suitable. In such cases, kurtosis can be used as a statistical index that gives different values from health to damage of a bearing and is, therefore, more suitable to measure the transients in the signal.

Spectral kurtosis (SK) for nonstationary signals is presented in [22]–[24]. The basic difference between kurtosis and SK is that kurtosis is computed over one frequency band, whereas SK is computed over each frequency band. Currently, several results in the literature have exemplified that the time-domain kurtosis, frequency-domain kurtosis, and SK can better distinguish the healthy and faulty bearing due to their property of determining the spikes in the vibration signals [24]–[26]. Moreover, if the faulty vibration signal is subjected to high noise as represented by (1), then kurtosis or SK fails to diagnose the faults of cyclostationary signals. In that case, a bandpass filter can be applied to the faulty signal to filter out the background noise of harmless vibration S_n and then kurtosis or SK can be computed to detect the fault frequency resonance band. However, parameters of the bandpass filter such as the center frequency and the bandwidth need to be selected for specific working conditions, making the filter effective only for those conditions. Different methods are proposed to improve the bandpass filter such as enhanced kurtogram [25] and fast kurtogram [26]. In an enhanced kurtogram, the vibration signal is decomposed to different depths, and kurtosis is calculated based on the power spectrum of the envelope of the decomposed signals. Whereas in a fast kurtogram, the vibration signal is decomposed with a 1/3 binary tree algorithm, and kurtosis is calculated using the short-time Fourier transform (STFT). In both methods, the resultant parameters of the bandpass filter such as central frequency and bandwidth are static and, therefore, it is highly possible for the filtered signal to miss the fault frequency spectrum and fail to diagnose the faults.

Motivated by the aforementioned literature, this article proposes an alternative method to design the improved bandpass filter that can vary its central frequency and bandwidth according to the fault frequency spectrum and external noises with alternative working conditions. The main contributions of this article include a new early-stage fault detection algorithm in which the signal-to-noise ratio of the faulty vibration signal is improved. Different from the enhanced kurtogram and fast kurtogram methods, the proposed method utilized the improved harmony search (HS) algorithm [27], [28] to optimize the parameters of the dynamic bandpass filter using different fitness functions based on kurtosis and SK. The values of these fitness functions increase from healthy to faulty signals. Using this attribution of fitness functions, optimum bandpass filters are constructed for each fitness function. The proposed method is fully data-driven that uses different datasets. The detail of the utilized datasets is mentioned in Section IV. The results of the proposed method are also compared with the fast kurtogram-based bandpass filter and it is concluded that the proposed method improves the power of the signal and enhances the fault frequency that helps to diagnose the faults more efficiently.

The rest of this article is arranged as follows. In Section II, the theoretical background for the fitness functions and the HS algorithm are reviewed. In Section III, the proposed algorithm is presented. In Section IV, different faulty vibration signals are used to diagnose the faults using the proposed method, and simulation and results are given. Section V consists of the conclusion.

II. Theoretical Background

In this section, different fitness functions and the HS algorithm are reviewed. The fitness functions used in this article are composed of kurtosis and SK.

A. Kurtosis

Kurtosis is a statical feature of the probability density function (PDF) to determine the strength of transient impulses of the nonstationary signal. In statistics, kurtosis can be defined as the fourth standardized moment [22], [26]. For a signal x with N number of samples and $\bar{x}$ sample means, the kurtosis is given as follows:

$$K = \frac{\frac{1}{N}\sum_{i=1}^{N}(x_i - \bar{x})^4}{\left(\frac{1}{N}\sum_{i=1}^{N}(x_i - \bar{x})^2\right)^2}. \tag{4}$$

When faults take place in a bearing, high-frequency transient impulses generated periodically raise the value of the kurtosis. Using this phenomenon, transient faults can be determined and the bearing faults can be diagnosed. By simple calculation, the kurtosis cannot distinguish between the noise and the fault impulses, and it is difficult to characterize the resonant band of the filtered signal.

B. Spectral Kurtosis

SK describes the kurtosis over each frequency band and allows to discover hidden transients and frequency bands in which these transients occur. We can calculate the SK value for the nonstationary signal in the presence of noise as follows:

$$K_{x+n}(f) = \frac{K_x(f)}{[1 + \rho(f)\ ]^2} \tag{5}$$

where $\rho(f)$ is the function of frequency representing the noise-to-signal ratio and $K_x(f)$ is the SK without noise. The latter can be given as the fourth-order normalized cumulant

$$K_x(f)\ = \frac{\lim_{x\to\infty}\frac{1}{N}\sum_{i=1}^{N}|H(n,f)|^4}{\left(\lim_{x\to\infty}\frac{1}{N}\sum_{i=1}^{N}|H(n,f)|^2\right)^2} - 2 \tag{6}$$

where $H(n, f)$ is the complex envelope of $x(n)$. The relationship between the signal $x(n)$ and complex envelop $H(n, f)$ is given by the following equation:

$$x(n) = \int_{+1/2}^{-1/2} H(n,f)e^{j2\pi fn}dZ_n(f). \tag{7}$$

C. STFT-Based SK

In (6), the complex envelope $H(n, f)$ is the function of time and frequency. The stochastic process $x(n)$ in (7) is characterized by a double stochasticity, both in $H(n, f)$ and $dZ_n(f)$. STFT is an efficient tool that can estimate better results and in the proposed algorithm, and $H(n, f)$ is replaced with STFT. For any stochastic process $x(n)$ with given analysis window $w(n)$ of length N, the STFT of $x(n)$ is defined as follows [22], [24], [29]:

$$\mathrm{STFT}(k, f) = \sum_{n=1}^{N} x(n) w(n-k) e^{-j2\pi nf} \tag{8}$$

where $w(n-k)$ is the short-time window with the shift k. The STFT-based SK is given by the following equation:

$$\mathrm{SK}_{\mathrm{STFT}} = \frac{\lim_{x\to\infty} \frac{1}{N} \sum_{i=1}^{N} |\mathrm{STFT}|^4}{\left(\lim_{x\to\infty} \frac{1}{N} \sum_{i=1}^{N} |\mathrm{STFT}|^2\right)^2} - 2. \tag{9}$$

D. HS Algorithm

The HS algorithm was inspired by the music-based metaheuristic optimization algorithm that was first introduced in 2011 [27]. The population of the HS algorithm consists of different musical sounds, and the aim is to find the best state of harmony. The optimization problem of a given function, subjected to the constraints is defined as

$$\begin{aligned} &\max f(X) \text{ or } \min f(X) \\ &\text{subjected to } g(X) \le 0 \quad \text{and} \quad h(X) = 0 \end{aligned} \tag{10}$$

where X is the set of solution candidates and the goal is to find the best solution candidate that optimizes (10), also called the fitness function.

There are three main key parameters of the HS algorithm that are described as follows.

1) Harmony memory size (HMS) or the number of solution candidates.
2) Harmony consideration rate (HMCR).
3) Pitch adjustment rate (PAR).

Generally, the values to these three key components are assigned in the following range [30] $10 \le \mathrm{HMS} \le 50$, $0.7 \le \mathrm{HMCR} \le 0.95$, and $0.2 \le \mathrm{PAR} \le 0.5$. The HS algorithm consists of the following five steps. In the first step, the specifying parameters, including the fitness function along with the constraints are defined, according to (10), and specific values are assigned to the three main parameters, that is, HMS, HMCR, and PAR. In the second step, a random harmony memory (HM) of order HMS $\times$ N is generated according to the following equation:

$$\mathrm{HM} = \begin{bmatrix} x_1^1 & x_2^1 & \cdots & x_N^1 \\ x_1^2 & x_2^2 & \cdots & x_N^2 \\ \vdots & \vdots & \ddots & \vdots \\ x_1^{\mathrm{HMS}} & x_2^{\mathrm{HMS}} & \cdots & x_N^{\mathrm{HMS}} \end{bmatrix} \tag{11}$$

where x_i^j, $i \in \mathrm{HMS}$, $j \in N$, is the element of the solution candidates $x^j = x_1^j, x_2^j, x_3^j, \ldots x_N^j$, and N is the number of elements in each solution candidate. Each element x_i^j of the solution candidate is bounded with upper bound x_{ub} and lower bound x_{lb} as follows:

$$x_{\mathrm{lb}} \le x_i^j \le x_{\mathrm{ub}}. \tag{12}$$

The fitness value is calculated using (10) for each solution candidate and the worst fitness value is determined. In the third step, a new harmony solution x_{new} is generated and its fitness value is calculated using (10). In the literature, different techniques are reported to generate the new harmony solution x_{new}. In general,

$$x_{\mathrm{new}} = \begin{cases} x_i^j \text{ from HM with probability HMCR} \\ \text{New solution with probability } (1 - \mathrm{HMCR}) \end{cases} \tag{13}$$

and then PAR for pitch adjustment is applied to x_{new}, as follows:

$$x_{\mathrm{new}} = \begin{cases} x_{\mathrm{new}} \pm\ bw \text{ with probability PAR} \\ x_{\mathrm{new}} \text{ with probability } (1 - \mathrm{PAR}) \end{cases} \tag{14}$$

where $bw = r \times (x_{\mathrm{ub}} - x_{\mathrm{lb}})$ and r is a positive random number such that $0 < r < 1$.

In the fourth step, the fitness values of x_{new} and the worst solution x^j from HM are compared. If the fitness value of x_{new} is better than the worst fitness value, then HM is updated by replacing the worst solution candidate x^j with x_{new}; otherwise, x_{new} is discarded.

In the fifth step, steps three and four are repeated until the stopping criteria or termination conditions are achieved. Finally, the best solution candidate is determined. This best solution candidate fulfills the optimization problem.

III. Proposed Method

Kurtosis and SK are efficient tools that vary their values from normal to faulty vibration signals and hence, fault can be diagnosed. But when the vibration signal is subjected to the high noise as given in (1), the kurtosis and SK are inefficient, and finding the fault frequency in the spectrum for a nonstationary signal is challenging because of the unwanted noise. To enhance the signal-to-noise ratio, a bandpass filter centered around the fault signal frequency is necessary. Because of the randomness of the fault frequency, a dynamic filter that can adjust its bandwidth and central frequency, depending on the processed signal, is needed.

In the proposed method, the HS algorithm is employed to optimize the bandpass filter using the different fitness functions based on kurtosis and SK. The fitness functions used to detect early-stage faults are: 1) kurtosis of the time-domain vibration signal; 2) kurtosis of the envelope spectrum of the vibration signal; and 3) sum of the STFT-based SK. The results of all three fitness functions are compared for the different faulty signals.

For that, fitness values of all the solution candidates from the randomly initialized HM [see (11)] are computed. The solution candidate with the highest fitness value is the best solution and vice versa. Then, using the HS algorithm, HM is improved by generating new solutions and computing the fitness values. This process is repeated for each subsequent epoch, until the stopping criteria are reached. At the end of the HS algorithm, the solution candidate with the highest fitness value is the

Algorithm 1 Bandpass Filter Design Using Improved HS Algorithm

Input : Fitness Function, HMS, HMCR, PAR, initial HM
Output: Bandpass Filter (central frequency, bandwidth, filter order)

```
// Main loop
for i ← 1 to max. no. of epoch do
    Construct BPF using updated HM and filter out vibration signal;
    Evaluate fitness value of each filtered signal
    if j < max. no. of solution candidates then
        // x_new generation
        if rand > HMCR then
            Generate x_new by random selection from HM
        else
            Generate x_new randomly within limits
        end if
        // Pitch adjustment of x_new
        if rand > PAR then
            Adjust the pitch of x_new
        else
            Keep x_new unchanged
        end if
    else
        // Offspring's Matrix
        ;
        Built offspring's Matrix;
        Construct BPF using offspring matrix and apply to vibration signal;
        Evaluate fitness value of each filtered signal;
        Accept x_new if better and update HM, otherwise discard x_new;
    end if
    Find the current best solutions;
end for
// Optimized Bandpass Filter
Find the best solution
Construct the Bandpass filter
Filtered out the vibration signal
Plot Envelope Spectrum and visualize the fault frequency
```

best solution. From that best solution, the bandpass filter is constructed and faults are diagnosed. The overall flow diagram for the proposed algorithm is depicted in Fig. 1. The three main key parameters HMS, HMCR, and PAR are chosen as 20, 0.72, and 0.08, respectively. The pseudocode for the modified HS algorithm for the proposed algorithm is given below.

IV. Simulations and Results

To validate the proposed method, two datasets were tested and the results were generated using the MATLAB environment. The first dataset was an intelligent maintenance system (IMS) bearing the dataset for test-to-failure vibration signal [31] and the second dataset was machinery failure prevention technology (MFPT) bearing the fault dataset [32].

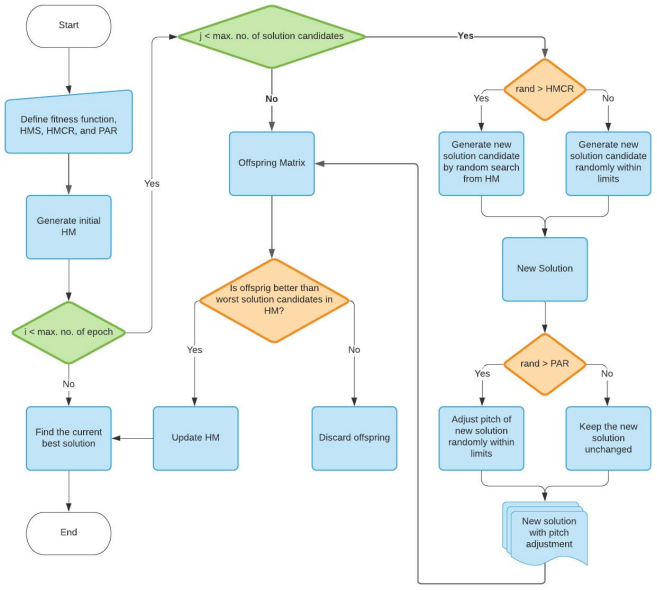

Fig. 1. Flow diagram of the proposed method.

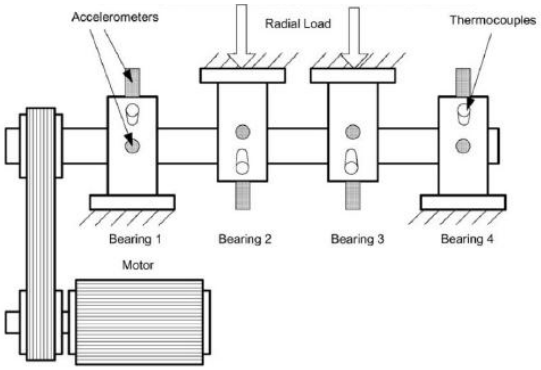

Fig. 2. Setup of test-to-failure experiment [33].

TABLE I
Test-to-Failure Bearing Specification

Description	Variable	Value
No. of rolling element bearings	n	16
Diameter of rolling elements	d	0.331
Pitch diameter of bearing	D	2.815
Bearing contact angle	α	15.17

Different vibration signals from these two datasets were taken to detect the fault frequencies. The detailed results are shown in Sections IV-A and IV-B.

A. Test-to-Failure Vibration Signal

To generate the datasets for test-to-failure vibration signal [31], [33], an ac motor with 2000 RPM constant speed was coupled to the shaft having four bearings and 6000 lbs radial load was applied by a spring mechanism as shown in Fig. 2. The vibration data was recorded for 1 s at specific intervals. The specification of the bearing is given in Table I.

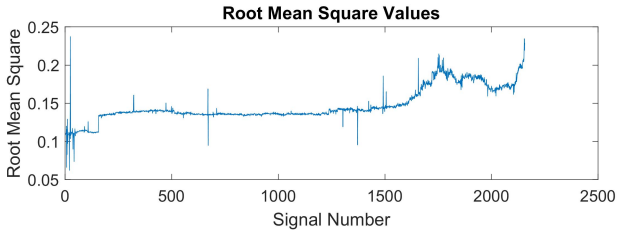

Fig. 3. RMS values of bearing 3 with roller element fault.

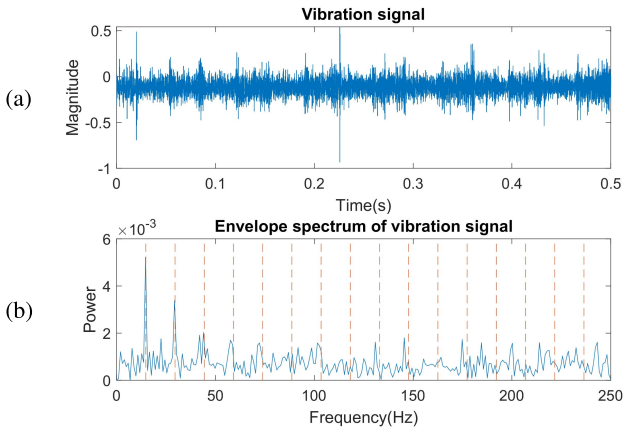

Fig. 4. Vibration signal 1515 with early-stage roller element fault. (a) Time plot. (b) Envelope spectrum.

Each data file comprises 20 480 points with 20-kHz sampling rate. The life of the bearing is 100 million revolutions and after this life, faults occur in the bearing. To validate the performance of the proposed method, we considered roller element fault and outer race fault from the test-to-failure dataset. Fig. 3 shows the root mean square (rms) plot of each data file of bearing 3 throughout the experiment. At the end of the experiment, roller element fault occurred in bearing 3 with a fault characteristic frequency of 14.7752 Hz.

It can be visualized from the rms values that file number 1515 has a high value which means the signal is faulty. Fig. 4 depicts the time-domain vibration signal and its envelope spectrum, respectively.

The power of the fault frequency could be enhanced if the unwanted signals are filtered out from faulty signals, as shown in Fig. 4(a). The bandpass filters were constructed using the proposed method and fast kurtogram method and results were compared to verify the performance of the proposed method. The parameters of the three bandpass filters designed using the proposed method are given below.

1) *Bandpass filter 1:* Center frequency = 2687.6 Hz; bandwidth = 1118.7 Hz; order of the filter = 46.
2) *Bandpass filter 2:* Center frequency = 1531 Hz; bandwidth = 843.6874 Hz; order of the filter = 61.
3) *Bandpass filter 3:* Center frequency = 3852 Hz; bandwidth = 3132.3 Hz; order of the filter = 88.

The faulty signals were filtered by the proposed method and their envelope spectrums are depicted in Fig. 5. The first fitness function is referred to as the time domain because it measures

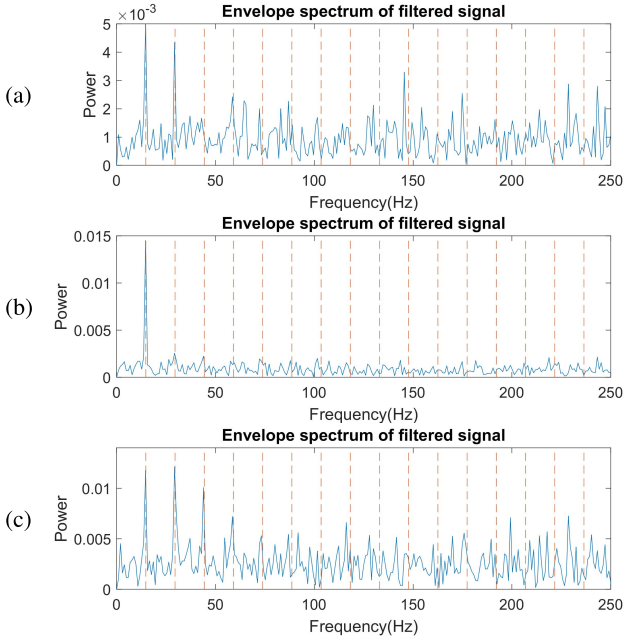

Fig. 5. Envelope spectrum of vibration signal 1515 with roller element fault. (a) Filtered using fitness function (1). (b) Filtered using fitness function (2). (c) Filtered using fitness function (3).

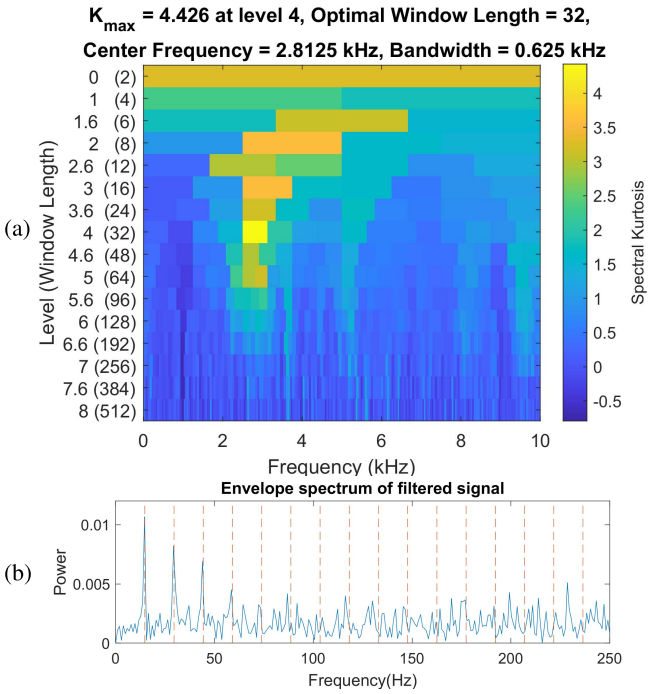

Fig. 6. Vibration signal 1515 with early-stage roller element fault. (a) Fast kurtogram. (b) Envelope spectrum.

the kurtosis of the time-domain signal, whereas the other two fitness functions are frequency domain. From the results, it was concluded that the frequency-domain fitness functions are better than the time-domain fitness function because they estimate the bandpass filter more efficiently.

A bandpass filter was constructed using the fast kurtogram shown in Fig. 6(a). The envelope spectrum of the filtered

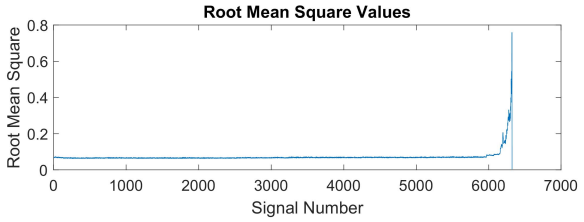

Fig. 7. RMS values of bearing 3 with outer race fault.

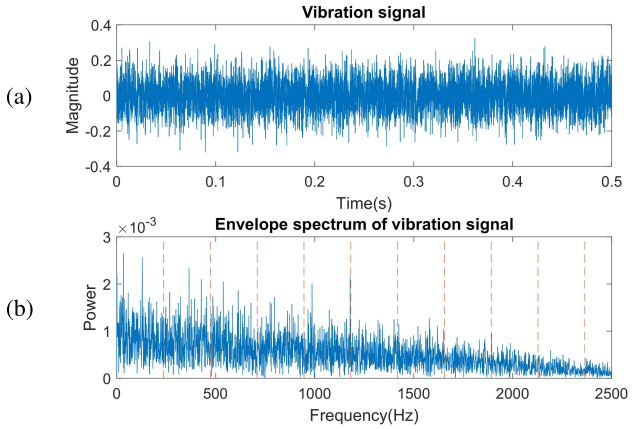

Fig. 8. Vibration signal 6100 with early-stage outer race fault. (a) Time plot. (b) Envelope spectrum.

signal improved the power of the fault frequency as shown in Fig. 6(b). When this result was compared with the proposed method, it was concluded that the proposed method is better. It is noted that the signal employed in this example was not taken from the early-stage fault region and therefore the unfiltered envelope spectrum shows the fault frequency. From this example, it can be concluded that the proposed method improves the power of the fault frequency and visualization. In the next example, we considered early-stage outer race fault signals and examined the validity of the proposed method. Outer race fault appeared with the fault characteristic frequency 236.4035 Hz in bearing 3. The rms plot of all the files is depicted in Fig. 7.

From the rms values, it can be seen that file number 6100 is within the early-stage fault. Therefore, this file or signal was taken to validate the proposed method. Fig. 8 shows the vibration signal 6100 and its envelope spectrum.

Due to the early-stage fault, the power of the faulty signal is very low and could not distinguish from the noise in the envelope spectrum in Fig. 8(b). To increase the signal-to-noise ratio and diagnose the early-stage fault, following three bandpass filters were constructed using the proposed method.

1) *Bandpass filter 1:* Center frequency = 3963.2 Hz; bandwidth = 2367.1 Hz; order of the filter = 98.
2) *Bandpass filter 2:* Center frequency = 3709.5 Hz; bandwidth = 1402.1 Hz; order of the filter = 46.
3) *Bandpass filter 3:* Center frequency = 2943.1 Hz; bandwidth = 4699.4 Hz; order of the filter = 67.

Fig. 9 shows the envelope spectrums of the filtered signal where early-stage outer race fault is clearly visualized.

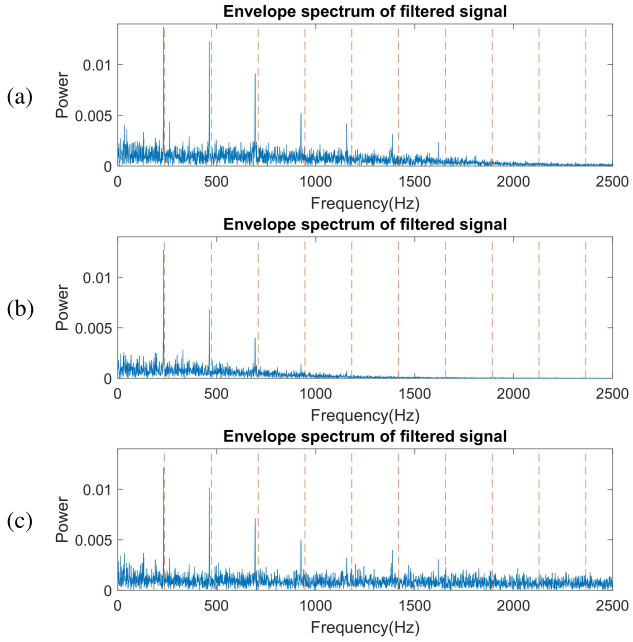

Fig. 9. Envelope spectrum of vibration signal 6100 with outer race fault. (a) Filtered using fitness function (1). (b) Filtered using fitness function (2). (c) Filtered using fitness function (3).

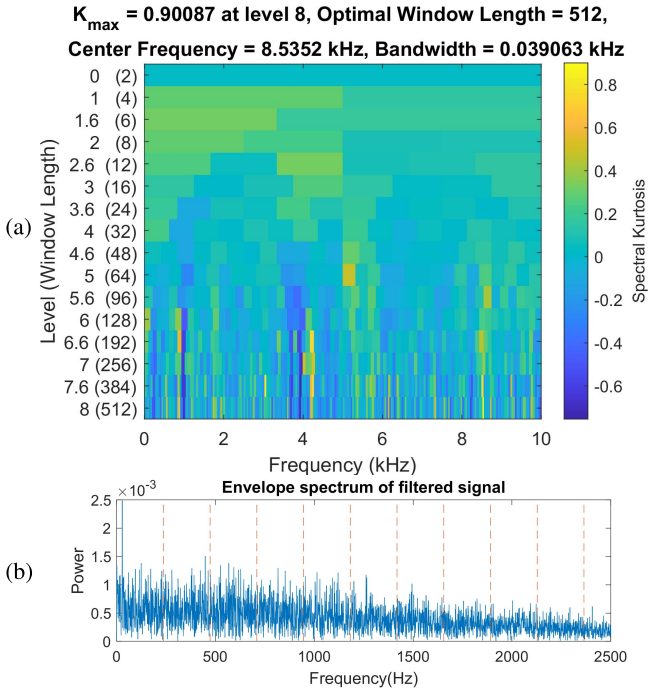

Fig. 10. Vibration signal 6100 with early-stage outer race fault. (a) Fast kurtogram. (b) Envelope spectrum.

Fig. 10 shows the fast kurtogram and envelope spectrum of the filtered signal. The power of the fault frequency in the early-stage signal is very low, and therefore, fault frequency cannot visualize in the envelope spectrum in Fig. 8(b). Moreover, the traditional method is inefficient to construct an accurate bandpass filter, and therefore, the envelope spectrum in Fig. 10(b) could not distinguish fault frequency. Consequently,

TABLE II
NICE BEARING SPECIFICATION

Description	Variable	Value
No. of rolling element bearings	n	8
Diameter of rolling elements	d	0.235
Pitch diameter of bearing	D	1.245
Bearing contact angle	α	0

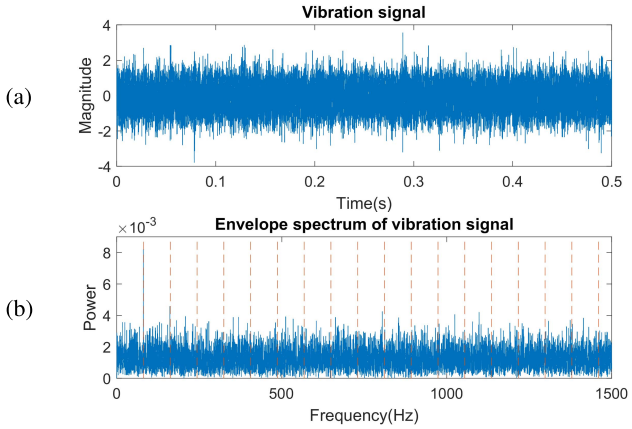

Fig. 11. Vibration signal (1) with outer race fault. (a) Time plot. (b) Envelope spectrum.

it can be concluded that the proposed method is efficient to diagnose early-stage faults.

B. MFPT Bearing Fault Dataset

The MFPT dataset with different loads was assembled [32]. The main purpose of this dataset is to improve the bearing analysis algorithms, research, and develop new techniques. To generate the dataset, a test rig with a NICE bearing was used. The bearing specification is presented in Table II.

From the MFPT dataset, we considered two highly noisy outer race fault signals and verified the performance of the proposed method to enhance the power of the fault frequency. The fault characteristic frequency for both signals is 81.1245 Hz. The time-domain vibration signal and its envelope spectrum of the first faulty signal are depicted in Fig. 11. From the envelope spectrum, it is difficult to visualize the fault frequency, and therefore, a bandpass filter is required to filter out the unwanted noise.

To compare the results of the proposed method with the traditional method, bandpass filters were optimized using the kurtosis and SK-based fitness functions as follows.

1) *Bandpass filter 1:* Center frequency = 3854.6 Hz; bandwidth = 1050.4 Hz; order of the filter = 95.
2) *Bandpass filter 2:* Center frequency = 2865 Hz; bandwidth = 4946 Hz; order of the filter = 60.
3) *Bandpass filter 3:* Center frequency = 2351.9 Hz; bandwidth = 3392.2 Hz; order of the filter = 61.

Fig. 12 shows the envelope spectrum of the filtered signal. It can be concluded that the signal-to-noise ratio is enhanced, and visualization of the fault frequency is improved.

Fig. 13 shows the fast kurtogram and envelope spectrum of the filtered signal. Comparing Fig. 13(b) with Fig. 12, it can

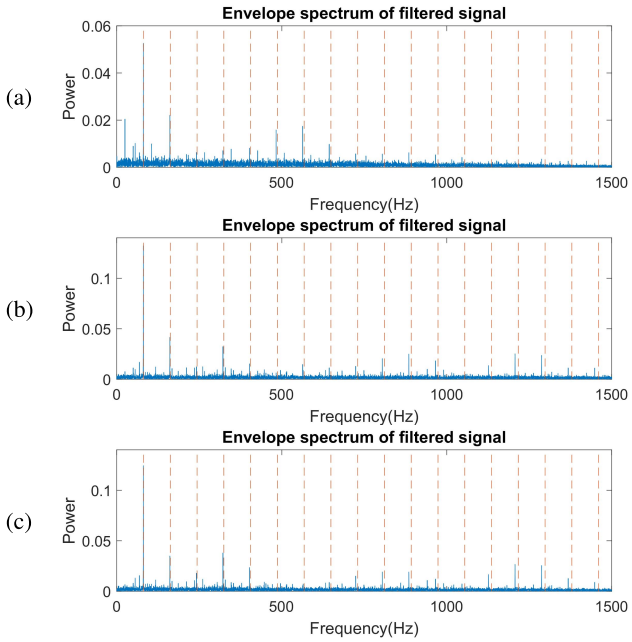

Fig. 12. Envelope spectrum of the vibration signal (1) with outer race fault. (a) Filtered using fitness function (1). (b) Filtered using fitness function (2). (c) Filtered using fitness function (3).

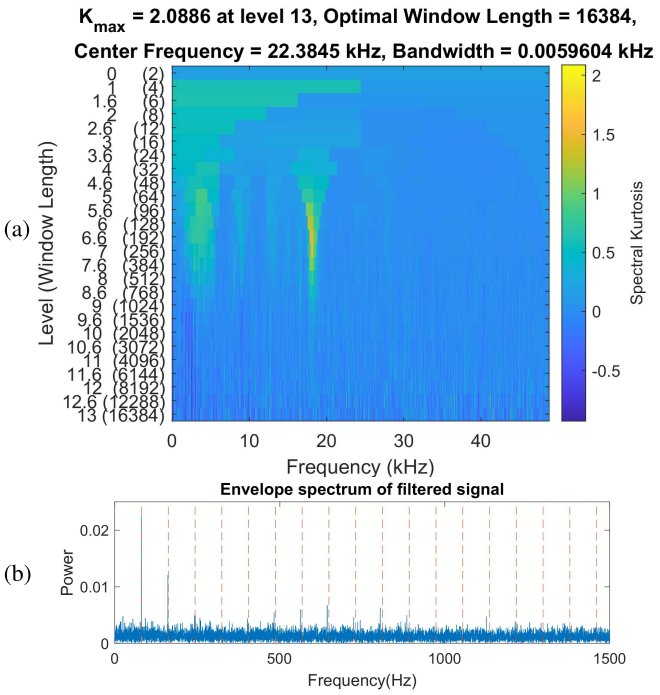

Fig. 13. Vibration signal (1) with outer race fault. (a) Fast kurtogram. (b) Envelope spectrum.

be concluded that the proposed method is more efficient to visualize the fault frequency.

Fig. 14 shows the second outer race fault signal and its envelope spectrum. The envelope spectrum of this signal does not show any fault frequency due to the high noise level. Following are the parameters of the bandpass filters designed using the proposed method.

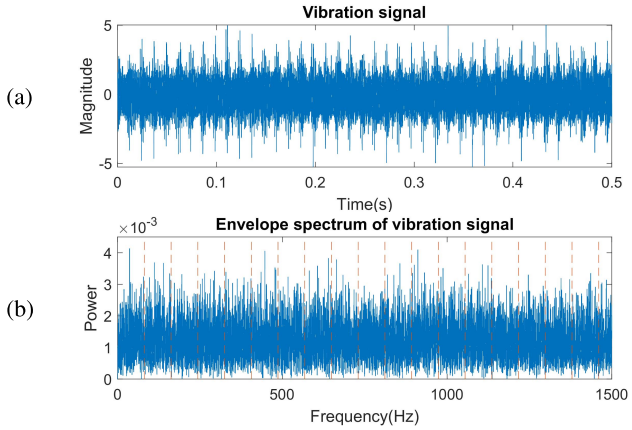

Fig. 14. Vibration signal (2) with outer race fault. (a) Time plot. (b) Envelope spectrum.

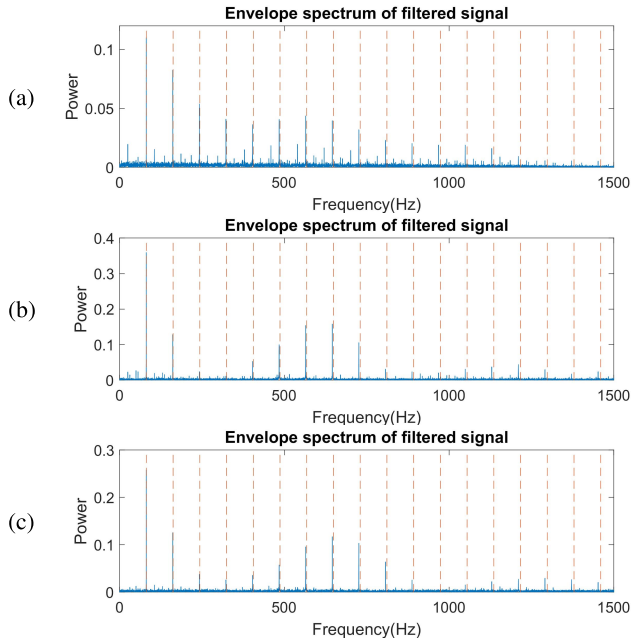

Fig. 15. Envelope spectrum of the vibration signal (2) with outer race fault. (a) Filtered using the fitness function (1). (b) Filtered using fitness function (2). (c) Filtered using fitness function (3).

1) *Bandpass filter 1:* Center frequency = 10 862 Hz; bandwidth = 1377.3 Hz; order of the filter = 99.
2) *Bandpass filter 2:* Center frequency = 24 415 Hz; bandwidth = 48 826 Hz; order of the filter = 97.
3) *Bandpass filter 3:* Center frequency = 6913 Hz; bandwidth = 10 218 Hz; order of the filter = 75.

Similar to the previous results, it can be concluded from Figs. 15 and 16(b) that the bandpass filters designed using the proposed method with frequency-domain fitness functions are more efficient than the time-domain fitness function as well as the fast kurtogram-based bandpass filter.

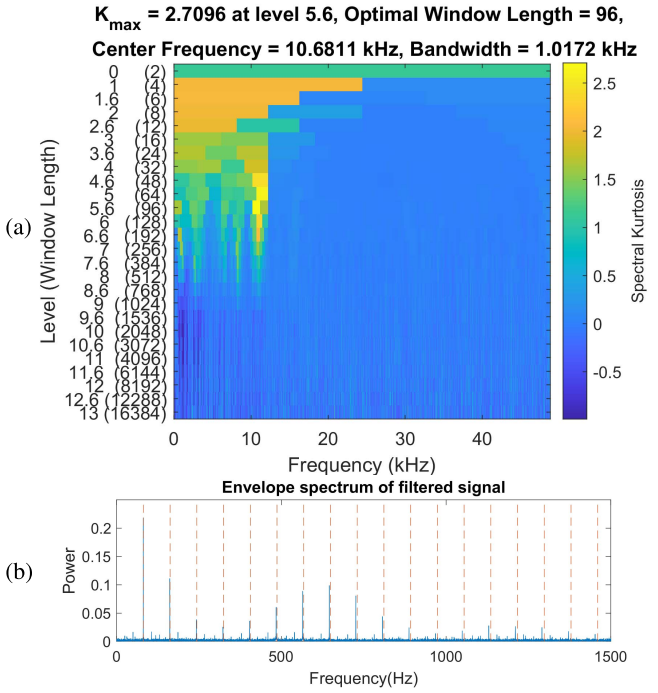

Fig. 16. Vibration signal (2) with outer race fault. (a) Fast kurtogram. (b) Envelope spectrum.

V. Conclusion

It is difficult to diagnose the faults from the early-stage vibration signals of the faulty bearings. Filtering out the vibration signal is an efficient tool to determine the fault frequencies, but it is challenging to estimate the optimized parameters for the bandpass filter. In this article, an improved HS algorithm is employed to estimate the dynamic parameters for the bandpass filter. Three different fitness functions based on kurtosis and SK are utilized to estimate the transients in the faulty vibration signals.

The resultant bandpass filters constructed with the help of kurtosis and SK-based fitness functions are compared with each other as well as with the fast kurtogram-based bandpass filter. It is concluded that the bandpass filters constructed using the frequency-domain fitness functions are efficient to diagnose the early-stage faults compared to the time-domain fitness function and fast kurtogram-based method. Frequency-domain fitness functions such as kurtosis of the envelope spectrum and STFT-based SK measure the transients in the frequency spectrums and hence are more efficient compared to the time-domain features. On the contrary, the kurtogram-based bandpass filter is constructed using the static tree algorithm and hence could fail to diagnose the fault frequency which can be seen in the simulation results.

References

[1] L. Wang, G. Cai, J. Wang, X. Jiang, and Z. Zhu, "Dual-enhanced sparse decomposition for wind turbine gearbox fault diagnosis," *IEEE Trans. Instrum. Meas.*, vol. 68, no. 2, pp. 450–461, Jul. 2019.

[2] G. Jiang, H. He, P. Xie, and Y. Tang, "Stacked multilevel-denoising autoencoders: A new representation learning approach for wind turbine gearbox fault diagnosis," *IEEE Trans. Instrum. Meas.*, vol. 66, no. 9, pp. 2391–2402, Sep. 2017.

[3] Q. He, J. Zhao, G. Jiang, and P. Xie, "An unsupervised multiview sparse filtering approach for current-based wind turbine gearbox fault diagnosis," *IEEE Trans. Instrum. Meas.*, vol. 69, no. 8, pp. 5569–5578, Aug. 2020.
[4] X. Yu, B. Tang, and K. Zhang, "Fault diagnosis of wind turbine gearbox using a novel method of fast deep graph convolutional networks," *IEEE Trans. Instrum. Meas.*, vol. 70, pp. 1–14, 2021.
[5] A. Rai and S. H. Upadhyay, "A review on signal processing techniques utilized in the fault diagnosis of rolling element bearings," *Tribol. Int.*, vol. 96, pp. 289–306, Apr. 2016. [Online]. Available: https://www.sciencedirect.com/science/article/pii/S0301679X15006052
[6] R. B. Randall and J. Antoni, "Rolling element bearing diagnostics-A tutorial," *Mech. Syst. Signal Process.*, vol. 25, no. 2, pp. 485–520, 2011. [Online]. Available: https://www.sciencedirect.com/science/article/pii/S0888327010002530
[7] S. Delvecchio, P. Bonfiglio, and F. Pompoli, "Vibro-acoustic condition monitoring of internal combustion engines: A critical review of existing techniques," *Mech. Syst. Signal Process.*, vol. 99, pp. 661–683, Jan. 2018. [Online]. Available: https://www.sciencedirect.com/science/article/pii/S088832701730345X
[8] D. Sun *et al.*, "On-line nonintrusive detection of wood pellets in pneumatic conveying pipelines using vibration and acoustic sensors," *IEEE Trans. Instrum. Meas.*, vol. 63, no. 5, pp. 993–1001, May 2014.
[9] D. Bismor, "Simulations of partial update LMS algorithms in application to active noise control," *Proc. Comput. Sci.*, vol. 80, pp. 1180–1190, 2016. [Online]. Available: http://www.sciencedirect.com/science/article/pii/S1877050916309358
[10] W. Wang, "Early detection of gear tooth cracking using the resonance demodulation technique," *Mech. Syst. Signal Process.*, vol. 15, no. 5, pp. 887–903, 2001. [Online]. Available: https://www.sciencedirect.com/science/article/pii/S0888327001914165
[11] A. Pries, D. Ramirez, and P. J. Schreier, "LMPIT-inspired tests for detecting a cyclostationary signal in noise with spatio–temporal structure," *IEEE Trans. Wireless Commun.*, vol. 17, no. 9, pp. 6321–6334, Sep. 2018.
[12] R.-B. Sun, F.-P. Du, Z.-B. Yang, X.-F. Chen, and K. Gryllias, "Cyclostationary analysis of irregular statistical cyclicity and extraction of rotating speed for bearing diagnostics with speed fluctuations," *IEEE Trans. Instrum. Meas.*, vol. 70, pp. 1–11, 2021.
[13] A. Soualhi, K. Medjaher, and N. Zerhouni, "Bearing health monitoring based on Hilbert–Huang transform, support vector machine, and regression," *IEEE Trans. Instrum. Meas.*, vol. 64, no. 1, pp. 52–62, Jan. 2015.
[14] W. Huang, G. Gao, N. Li, X. Jiang, and Z. Zhu, "Time-frequency squeezing and generalized demodulation combined for variable speed bearing fault diagnosis," *IEEE Trans. Instrum. Meas.*, vol. 68, no. 8, pp. 2819–2829, Aug. 2019.
[15] R. Yan and R. X. Gao, "Hilbert–Huang transform-based vibration signal analysis for machine health monitoring," *IEEE Trans. Instrum. Meas.*, vol. 55, no. 6, pp. 2320–2329, Dec. 2006.
[16] Q. B. He, H. Y. Song, and X. X. Ding, "Sparse signal reconstruction based on time-frequency manifold for rolling element bearing fault signature enhancement," *IEEE Trans. Instrum. Meas.*, vol. 65, no. 2, pp. 482–491, Feb. 2016.
[17] I. Attoui, N. Boutasseta, and N. Fergani, "Novel machinery monitoring strategy based on time–frequency domain similarity measurement with limited labeled data," *IEEE Trans. Instrum. Meas.*, vol. 70, pp. 1–8, 2021.
[18] D. Zhang, E. Stewart, J. Ye, M. Entezami, and C. Roberts, "Roller bearing degradation assessment based on a deep MLP convolution neural network considering outlier regions," *IEEE Trans. Instrum. Meas.*, vol. 69, no. 6, pp. 2996–3004, Jun. 2020.
[19] R. Zhang, H. Tao, L. Wu, and Y. Guan, "Transfer learning with neural networks for bearing fault diagnosis in changing working conditions," *IEEE Access*, vol. 5, pp. 14347–14357, 2017.
[20] M.-Q. Tran, M.-K. Liu, Q.-V. Tran, and T.-K. Nguyen, "Effective fault diagnosis based on wavelet and convolutional attention neural network for induction motors," *IEEE Trans. Instrum. Meas.*, vol. 71, pp. 1–13, 2022.
[21] D. Abboud, J. Antoni, S. Sieg-Zieba, and M. Eltabach, "Envelope analysis of rotating machine vibrations in variable speed conditions: A comprehensive treatment," *Mech. Syst. Signal Process.*, vol. 84, pp. 200–226, Feb. 2017. [Online]. Available: https://www.sciencedirect.com/science/article/pii/S088832701630214X
[22] S. S. Udmale and S. K. Singh, "Application of spectral kurtosis and improved extreme learning machine for bearing fault classification," *IEEE Trans. Instrum. Meas.*, vol. 68, no. 11, pp. 4222–4233, Nov. 2019.
[23] Y. Hu, W. Bao, X. Tu, F. Li, and K. Li, "An adaptive spectral kurtosis method and its application to fault detection of rolling element bearings," *IEEE Trans. Instrum. Meas.*, vol. 69, no. 3, pp. 739–750, Mar. 2020.
[24] J. Antoni, "The spectral kurtosis: A useful tool for characterising non-stationary signals," *Mech. Syst. Signal Process.*, vol. 20, no. 2, pp. 282–307, 2002. [Online]. Available: https://www.sciencedirect.com/science/article/pii/S0888327004001517
[25] D. Wang, P. W. Tse, and K. L. Tsui, "An enhanced Kurtogram method for fault diagnosis of rolling element bearings," *Mech. Syst. Signal Process.*, vol. 35, nos. 1–2, pp. 176–199, Feb. 2013. [Online]. Available: https://www.sciencedirect.com/science/article/pii/S0888327012003767
[26] J. Antoni, "Fast computation of the kurtogram for the detection of transient faults," *Mech. Syst. Signal Process.*, vol. 21, no. 1, pp. 108–124, 2007. [Online]. Available: https://www.sciencedirect.com/science/article/pii/S0888327005002414
[27] Z. W. Geem, J. H. Kim, and G. V. Loganathan, "A new heuristic optimization algorithm: Harmony search," *J. Simul.*, vol. 76, no. 2, pp. 60–68, Feb. 2001. [Online]. Available: www.scopus.com
[28] T. Zhang and Z. W. Geem, "Review of harmony search with respect to algorithm structure," *Swarm Evol. Comput.*, vol. 48, pp. 31–43, Aug. 2019. [Online]. Available: https://www.sciencedirect.com/science/article/pii/S2210650218303791
[29] F. Millioz and N. Martin, "Circularity of the STFT and spectral kurtosis for time-frequency segmentation in Gaussian environment," *IEEE Trans. Signal Process.*, vol. 59, no. 2, pp. 515–524, Feb. 2011.
[30] K. S. Lee, Z. W. Geem, S.-H. Lee, and K.-W. Bae, "The harmony search heuristic algorithm for discrete structural optimization," *Eng. Optim.*, vol. 37, no. 7, pp. 663–684, 2005, doi: 10.1080/03052150500211895.
[31] (2018). *Center for Intelligent Maintenance Systems (IMS), University of Cincinnati*. Prognostic Data Repository of NASA. [Online]. Available: https://ti.arc.nasa.gov/tech/dash/groups/pcoe/prognostic-data-repository/
[32] Mfpt Dataset. (2012). *Society for Machinery Failure Prevention Technology*. [Online]. Available: https://mfpt.org/fault-data-sets/
[33] H. Qiu, J. Lee, J. Lin, and G. Yu, "Wavelet filter-based weak signature detection method and its application on rolling element bearing prognostics," *J. Sound Vib.*, vol. 289, nos. 4–5, pp. 1066–1090, Feb. 2006.

Muhammad Ahsan received the M.Sc. degree in control theory and control engineering from the Nanjing University of Science and Technology, Nanjing, China, in 2020.

In October 2020, he has joined the Silesian University of Technology, Gliwice, Poland, where he has been working on digital signal processing and artificial intelligence methods for fault diagnosis in bearing and machine health monitoring. His research interests include digital signal processing, optimization, and nonlinear control.

Dariusz Bismor (Senior Member, IEEE) received the M.Sc. and Ph.D. degrees in control sciences from the Silesian University of Technology, Gliwice, Poland, in 1995 and 2000, respectively, and the Habilitation degree from the Department of Measurements and Control Sciences, Silesian University of Technology, in 2016.

Since 2017, he has been a Professor with the Department of Measurements and Control Sciences, Silesian University of Technology. He is the author of three books and numerous scientific articles. His scientific interests include digital signal processing, active noise control, system identification, adaptive control, control of industrial processes, and vibration diagnosis.

Dr. Bismor is a member of the Polish Acoustical Society (since 1997), European Acoustics Association (EAA), and International Institute of Acoustics and Vibration (IIAV). He is a Production Editor and a member of the Editorial Board of *International Journal of Acoustics and Vibration*.